IEEE Control Systems Letters paper presented at
2023 American Control Conference (ACC)
San Diego, CA, USA. May 31 - June 2, 2023

# Lyapunov-based Current-Profile Feedback Control in Tokamaks with Nonsymmetric Individual Actuator Saturation*

Sai Tej Paruchuri, Andres Pajares, and Eugenio Schuster

***Abstract*— Advanced tokamak scenarios can achieve optimal tokamak operation by shaping the plasma internal profiles through the use of noninductive heating and current sources. As a result of the dynamic complexities, active control of the power of each noninductive heating and current source, a non-negative value, may be necessary to achieve the desired tokamak performance. However, due to the inherent physical limitations, arbitrary power prescription by the controller may saturate the heating and current drives. Therefore, it is highly desirable to develop a class of active control algorithms that account for the saturation limits of these actuators. A Lyapunov-based nonlinear feedback control algorithm that intrinsically accounts for saturation limits is proposed in this work to regulate the spatial distribution of the toroidal current density in the tokamak. The controller does not rely on constrained optimization techniques, which can be computationally expensive for real-time implementation. Furthermore, the controller can handle nonsymmetric saturation limits, i.e., the absolute values of the upper and lower saturation limits do not have to be equal. The effectiveness of the control algorithm is demonstrated for a DIII-D tokamak scenario in nonlinear simulations.**

## I. INTRODUCTION

A *plasma* is a hot ionized gas composed of positively charged ions and negatively charged electrons. Since their composition comprises charged particles, external electric and magnetic fields can affect their behavior. *Tokamaks* are torus-shaped devices that use helical magnetic fields to confine the plasma at temperatures above ten times the sun's core temperature [1]. At these temperatures, ions possess enough kinetic energy to overcome the Coulombic forces of repulsion when they collide, and consequently they combine to form a larger nucleus. Such a reaction releases a large amount of energy and is called nuclear fusion. The primary emphasis of tokamak research is to develop economically sustainable means of energy production through nuclear fusion. Stable operation of tokamaks with steady plasma confinement is necessary to achieve nuclear fusion with high fusion gain, the ratio of energy produced through fusion to the input energy. Such tokamak operating conditions require maintaining several plasma properties at predetermined optimal levels. Deviation from these optimal levels can result in magnetohydrodynamic instabilities that can deteriorate or terminate plasma confinement. One such plasma parameter is the current flowing toroidally in the plasma, which is a continuous function of space and time, and its spatial variation results in what is referred to as the "current profile." Due to the model uncertainties and process noise, feedforward control of the current profile may not be sufficient in certain tokamak scenarios. In such cases, it may be necessary to implement active feedback control of the current profile.

Conventionally, noninductive current sources are used for extended tokamak operation in advanced tokamak (AT) scenarios. Such sources include neutral beam injector (NBI), electron cyclotron heating and current drive (ECH&CD). In this work, NBI and ECH&CD are considered controllable inputs during the controller synthesis. The implementation of control strategies without consideration of physical limits can potentially saturate the power of these sources.

In the last decade, researchers have extensively studied model-based current profile control using noninductive current drives. The feedback control methods used in the existing literature include proportional–integral–derivative (PID) control and its variants, where control models are used to define the state errors and PID gains, [2], backstepping control [3], passivity based control [4], and optimal feedback control (linear-quadratic regulator - LQR and linear-quadratic-integral control - LQI) [5], [6]. Before designing a finite-dimensional controller, the control models are discretized spatially in the above-cited literature. Alternatively, infinite-dimensional controllers with certain simplifying assumptions are presented in [7]. A bulk of these references do not account for saturation constraints of the noninductive current drives. One can potentially use an anti-windup or anti-saturation compensator to avoid integrator windup and prevent saturation of actuators. However, such compensators handle saturation a posteriori to the control block and are primarily effective only when the control algorithm includes integral action. On the other hand, one can consider the saturation limits in model predictive control (MPC) [8] or optimization-based feedback linearization control (which uses optimization to achieve nonlinearity cancellation) [9], [10]. In MPC, a finite horizon optimal control problem (FHOCP) is solved at each time step. Due to the high computational cost of solving the FHOCP, model simplification measures like linearization may be required to make experimental implementation feasible. Likewise, an optimization-based feedback linearization controller solves a finite-dimensional optimization problem at each time step. In some tokamak scenarios, the computational cost can be too high for plasma control applications. Therefore, implementing a *nonlinear feedback control* technique that implicitly considers the *actuator constraints* while avoiding the

*This material is based upon work supported by the U.S. Department of Energy, Office of Science, Office of Fusion Energy Sciences, under Award Numbers DE-SC0010537 and DE-SC0010661. S.T. Paruchuri (saitejp@lehigh.edu) and E. Schuster are with the Department of Mechanical Engineering and Mechanics, Lehigh University, Bethlehem, PA 18015, USA. A. Pajares is with General Atomics, San Diego, CA 92121, USA.

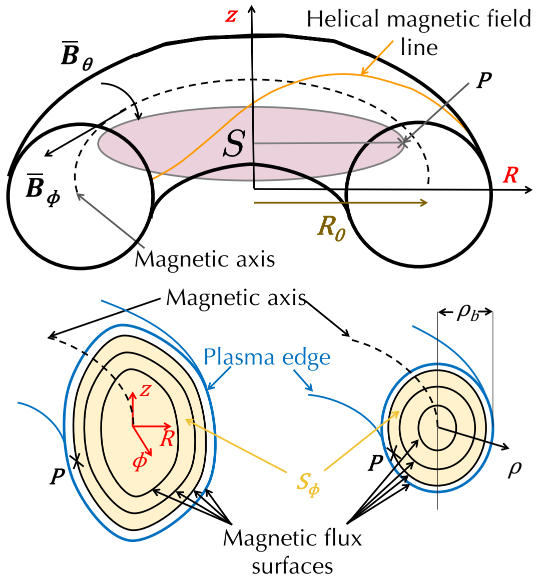


Fig. 1: Illustration of magnetic fields in a tokamak.

computational burden associated with real-time optimization can be advantageous for controlling the current profile using noninductive current drives.

This paper presents a nonlinear Lyapunov-based feedback controller that inherently accounts for the nonsymmetric saturation limits of each actuator. In particular, the proposed controller does not require solving any optimization problem, which significantly reduces computational complexity. The controller proposed in this work can be considered as an extension of the modified Sontag's controller [11], which is designed to control a specific class of nonlinear systems while accounting for saturation limits. The primary difference between the cited reference and this work is that the controller proposed in the literature ensures that the input vector's norm is bounded from above by a constant. However, it does not place any bounds on individual input values. Choosing the minimum of the actuators' saturation limits as the upper bound can prevent saturation of all the inputs. However, such a selection constrains the controller capabilities. Furthermore, the controllers in the cited literature cannot be implemented in cases where the saturation limits are not symmetrical, i.e., the absolute value of the upper and lower saturation limits are not equal. In contrast, the controller proposed in this work ensures that each individual input is bounded from below and above by the lower and upper saturation limits, respectively.

This paper is organized as follows. Section II details the control-oriented plasma model that will be used for control synthesis. In particular, the section describes the assumptions and the tokamak's setting required for implementing the controller. Section III rigorously goes over the steps involved in the control design. Section IV presents some nonlinear simulation results. The conclusion of this work and potential future work are given in Section V.

## II. Plasma Model

The helical magnetic field $\bar{B}$ in a tokamak is made up of the toroidal and the poloidal magnetic fields, $\bar{B}_\phi$ and $\bar{B}_\theta$, that are generated by the toroidal and the poloidal field coils, respectively (refer to Figure 1). The poloidal magnetic flux at any given point $P$ in the tokamak is defined as $\Psi := \int_S \bar{B}_\theta \cdot d\bar{S}$. The term $S$ is the toroidal surface normal to the axis $z$ and is formed by the circle passing through the point $P$ (refer to Figure 1). Under ideal MHD conditions, the poloidal magnetic flux surfaces (set of points with constant poloidal magnetic flux) form nested surfaces as shown in Figure 1. Any term that indexes the flux surfaces can be used as a spatial variable while modeling the plasma dynamics. In this work, the normalized mean effective minor radius $\hat{\rho} \in [0, 1]$ is used as the spatial variable. It is crucial to understand that $\hat{\rho}$ is not a measure of tokamak's radius in the conventional sense. Note that the axial symmetry assumption along with the nested magnetic flux surfaces reduce the dimension of the spatial variable from three to one. By definition, the spatial variable $\hat{\rho}$ is given by $\hat{\rho} := \rho/\rho_b$. The term $\rho$ is the mean effective minor radius and is defined as $\rho := \sqrt{\Phi/B_{\phi,0}\pi}$, where $\Phi$ is the toroidal magnetic flux, and $B_{\phi,0}$ is the vacuum toroidal magnetic field at the major radius $R_0$. The term $\rho_b$ in the definition of $\hat{\rho}$ is the mean effective minor radius at the last closed magnetic flux surface. The toroidal current density $j_{tor}$ is defined as

$$j_{tor}(\hat{\rho}, t) := -\frac{1}{\mu_0 \rho_b^2 R_0 \hat{H}} \frac{1}{\hat{\rho}} \frac{\partial}{\partial \hat{\rho}} \left( \hat{\rho} \hat{G} \hat{H} \frac{\partial \psi}{\partial \hat{\rho}} \right). \tag{1}$$

In the above equation, the terms $t$ and $\mu_0$ are the time and vacuum permeability, respectively. The terms $\hat{G}$, $\hat{H}$ are functions of the spatial variable $\hat{\rho}$ and depend on the plasma shape. It is clear from the above definition that $j_{tor}$ depends on the gradient of poloidal stream function $\psi := \Psi/2\pi$. Thus, controlling the gradient of the poloidal stream function is equivalent to regulating the toroidal current density.

The magnetic diffusion equation [12] is given by

$$\frac{\partial \psi}{\partial t} = \frac{\eta}{\mu_0 \rho_b^2 \hat{F}^2} \frac{1}{\hat{\rho}} \frac{\partial}{\partial \hat{\rho}} \left( \hat{\rho} D_\psi \frac{\partial \psi}{\partial \hat{\rho}} \right) + R_0 \hat{H} \eta j_{ni}, \tag{2}$$

and the corresponding boundary conditions are

$$\left.\frac{\partial \psi}{\partial \hat{\rho}}\right|_{\hat{\rho}=0} = 0, \qquad \left.\frac{\partial \psi}{\partial \hat{\rho}}\right|_{\hat{\rho}=1} = -\underbrace{\frac{\mu_0}{2\pi} \frac{R_0}{\hat{G}_{\hat{\rho}=1} \hat{H}_{\hat{\rho}=1}}}_{k_{I_p}} I_p. \tag{3}$$

In the above equation, the terms $I_p$, $\eta$ and $j_{ni}$ are the plasma current, plasma resistivity and non-inductive current, respectively. The term $\hat{F}$ is a function of the spatial variable $\hat{\rho}$ and depends on the plasma shape. The function $D_\psi$ of $\hat{\rho}$ is defined as $D_\psi := \hat{F}\hat{G}\hat{H}$. Both plasma resistivity $\eta$ and noninductive current $j_{ni}$ exhibit complex dynamics that require high-fidelity models. However, consideration of such models makes the controller design complex, if not impossible. As a result, control-oriented models developed in [13] are used to model $\eta$ and $j_{ni}$ in this work. The control-oriented model for $\eta$ assumes that the electron-temperature in the tokamak evolves as the product of time-varying scalar and a fixed basis function. It is given by

$$\eta = Z_{eff} k_{sp} T_e^{-3/2} \approx g_\eta \times (I_p^\gamma P_{tot}^\epsilon \bar{n}_e^\zeta)^{-3/2}, \quad (4)$$

where $Z_{eff}$, $k_{sp}$ and $T_e$ are the effective atomic number of the plasma ions, a fixed spatial profile (function of $\hat{\rho}$) and the electron temperature, respectively. The terms $g_\eta$ is a function of $\hat{\rho}$, $P_{tot}$ is the total power, and $\bar{n}_e$ is the line-average electron density. In addition, the terms $\gamma$, $\epsilon$ and $\zeta$ are constant coefficients of the proposed scaling law. The control-oriented model for noninductive current $j_{ni}$ is given by

$$\begin{aligned}\eta j_{ni} \approx & \sum_{i=1}^{N_{NBI}} g_{NBI,i} \times (I_p^\gamma P_{tot}^\epsilon \bar{n}_e^\zeta)^{(-3/2+\epsilon_{NBI})} \bar{n}_e^{-1} P_{NBI,i} \\ & + g_{EC} \times (I_p^\gamma P_{tot}^\epsilon \bar{n}_e^\zeta)^{(-3/2+\epsilon_{EC})} \bar{n}_e^{-1} P_{EC} \\ & + (\partial\psi/\partial\hat{\rho})^{-1} g_{BS} \times (I_p^\gamma P_{tot}^\epsilon \bar{n}_e^\zeta)^{-1/2} \bar{n}_e.\end{aligned} \quad (5)$$

In the above equation, the terms $g_{NBI,i}$, $g_{EC}$, and $g_{BS}$ are function of $\hat{\rho}$ and account for the current deposition profiles of the neutral beam injector, electron cyclotron current and bootstrap current, respectively. The effect of the noninductive current drive on the plasma dynamics is captured by the above model. In this work, the tokamak is assumed to have $N_{NBI}$ NBIs and one ECH&CD. The terms $P_{NBI,i}$ and $P_{EC}$ correspond to the NBI and ECH&CD powers, respectively. Note that the bootstrap current is a self-generated current that is caused by the pressure gradient in the tokamak. The effect of the bootstrap current on the plasma dynamics is nonlinear. The constants $\epsilon_{NBI}$, $\epsilon_{EC}$ are the NBI and ECH&CD scaling coefficients, respectively.

In the context of this paper, the noninductive powers $P_{NBI,1}, \ldots, P_{NBI,N_{NBI}}, P_{EC}$ are considered the controllable inputs, i.e., they are prescribed by the current profile controller designed in the following section. On the other hand, the plasma current $I_P$, the line-average electron density $\bar{n}_e$, and the total power $P_{tot}$ are considered prescribed terms. Note that the total power $P_{tot}$ is given by the expression

$$P_{tot} = \sum_{i=1}^{N_{NBI}} P_{NBI,i} + P_{EC} + \sum_{j=1}^{N_o} P_j, \quad (6)$$

where $P_j$ corresponds to the power injected by $N_o$ additional actuators that are tuned to heat the plasma instead of driving a net current. As a result, these actuators are not included in the model for noninductive current given in (5). Typically, the value of $P_{tot}$ is prescribed by a separate controller to track a reference plasma $\beta$ (ratio of the kinetic pressure to the magnetic pressure). Once the plasma $\beta$ controller and the current profile controller prescribe $P_{tot}$ and $P_{NBI,1}, \ldots, P_{NBI,N_{NBI}}, P_{EC}$, respectively, the assumption is that a separate algorithm allocates the values of $N_o$ heating actuators' powers such that the constraint given in (6) is satisfied. However, the design of the plasma $\beta$ controller and heating actuator power allocation algorithm is beyond the scope of the current work.

Generally, the target for current profile control is given in terms of the gradient of the poloidal stream function or its related quantities. Hence, it is beneficial to work with a model for control design that defines the evolution of the poloidal flux gradient $\theta$, which is defined as $\theta := \frac{\partial\psi}{\partial\hat{\rho}}$. Introducing the models for plasma resistivity (4) and noninductive current (5) in (2) and taking the derivative with respect to the spatial variable $\hat{\rho}$ results in the partial differential equation (PDE)

$$\begin{aligned}\dot{\theta} = & \left(h_{\eta,1}\theta'' + h_{\eta,2}\theta' + h_{\eta,3}\theta\right) u_\eta + h_{EC} u_{EC} \\ & + \sum_{i=1}^{N_{NBI}} h_{NBI,i} u_{NBI,i} + \left(h_{BS,1}\frac{1}{\theta} - h_{BS,2}\frac{\theta'}{\theta^2}\right) u_{BS}\end{aligned} \quad (7)$$

with the boundary conditions

$$\theta(0) = 0, \qquad \theta(1) = -k_{I_p} I_p. \quad (8)$$

The notations $\dot{(\cdot)}$ and $(\cdot)'$ in the above expressions represents the first derivative with respect to the time $t$ and spatial variable $\hat{\rho}$. In the above PDE, the terms $h_{\eta,1}$, $h_{\eta,2}$, $h_{\eta,3}$, $h_{NBI,i}$, $h_{EC}$, $h_{BS,1}$ and $h_{BS,2}$ are functions of $\hat{\rho}$ and are defined as

$$\begin{aligned}h_{\eta,1} &:= \frac{1}{\mu_0 \rho_b^2} \frac{g_\eta}{\hat{F}^2} D_\psi, \\ h_{\eta,2} &:= \frac{1}{\mu_0 \rho_b^2} \left[ \left(\frac{g_\eta}{\hat{F}^2}\right)' D_\psi + \frac{g_\eta}{\hat{F}^2} \left(\frac{D_\psi}{\hat{\rho}} + 2D'_\psi\right) \right], \\ h_{\eta,3} &:= \frac{1}{\mu_0 \rho_b^2} \left[ \left(\frac{g_\eta}{\hat{F}^2}\right)' \left(\frac{D_\psi}{\hat{\rho}} + D'_\psi\right) + \frac{g_\eta}{\hat{F}^2} \left(\frac{D'_\psi \hat{\rho} - D_\psi}{\hat{\rho}^2}\right) \right],\end{aligned}$$

$$h_{NBI,i} := R_0 \times (\hat{H} \times g_{NBI,i})', \qquad h_{EC} := R_0 \times (\hat{H} \times g_{EC})',$$
$$h_{BS,1} := R_0 \times (\hat{H} \times g_{BS})', \qquad h_{BS,2} := R_0 \times \hat{H} \times g_{BS}.$$

The terms $u_\eta$, $u_{NBI,i}$, $u_{EC}$ and $u_{BS}$ in the PDE shown in (7) are functions of time $t$ and are defined as

$$u_\eta := (I_p^\gamma P_{tot}^\epsilon \bar{n}_e^\zeta)^{-3/2}, \quad u_{BS} := (I_p^\gamma P_{tot}^\epsilon \bar{n}_e^\zeta)^{-1/2} \bar{n}_e, \quad (9)$$
$$u_{NBI,i} := (I_p^\gamma P_{tot}^\epsilon \bar{n}_e^\zeta)^{(-3/2+\zeta_{NBI})} \bar{n}_e^{-1} P_{NBI,i}, \quad (10)$$
$$u_{EC} := (I_p^\gamma P_{tot}^\epsilon \bar{n}_e^\zeta)^{(-3/2+\zeta_{EC})} \bar{n}_e^{-1} P_{EC}. \quad (11)$$

One can consider the above terms as virtual inputs as opposed to the actual physical inputs $P_{NBI,i}$ and $P_{EC}$.

Before deriving the error equations, the PDE given in (7) is approximated using a finite difference scheme. The spatial variable $\hat{\rho}$ is discretized with $N+1$ nodes $(\hat{\rho}_0, \ldots, \hat{\rho}_N)$ with a constant step size of $\Delta\hat{\rho} = 1/N$. The first and second order derivatives are approximated using the relations

$$\theta'_i(t) = \frac{\theta_{i+1}(t) - \theta_{i-1}(t)}{2\Delta\hat{\rho}}, \quad \theta''_i(t) = \frac{\theta_{i+1}(t) + \theta_{i-1}(t) - 2\theta_i(t)}{2\Delta\hat{\rho}^2}.$$

where $\theta_i(t) = \theta(\hat{\rho}_i, t)$. Using the above approximations for the derivatives in the PDE given in (7) results in the finite-dimensional ordinary differential equation (ODE)

$$\dot{\boldsymbol{\theta}}(t) = G_\eta(\boldsymbol{\theta}, t) u_\eta + G_{aux} \boldsymbol{u}_{aux} + G_{BS}(\boldsymbol{\theta}, t) u_{BS}, \quad (12)$$

where $\boldsymbol{\theta}(t) = [\theta(\hat{\rho}_1, t), \ldots, \theta(\hat{\rho}_{N-1}, t)]^T$, $\boldsymbol{u}_{aux} = [u_{NBI,1}, \ldots, u_{NBI,N_{NBI}}, u_{EC}]^T$, and the $m^{th}$ row of the terms $G_\eta(\boldsymbol{\theta}, t), G_{aux}, G_{BS}(\boldsymbol{\theta}, t)$ are given by

$$G_{\eta,m}(\boldsymbol{\theta}, t) = \alpha_m \theta_{m-1} + \beta_m \theta_{m+1} + \gamma_m \theta_m, \quad (13)$$
$$G_{aux,m} = [h_{NBI,1}^m, \ldots, h_{NBI,N_{NBI}}^m, h_{EC}^m], \quad (14)$$
$$G_{BS,m}(\boldsymbol{\theta}, t) = \frac{h_{BS,1}^m}{\theta_m} - \frac{h_{BS,2}^m}{\theta_m^2} \frac{\theta_{m+1} - \theta_{m-1}}{2\Delta\hat{\rho}} \quad (15)$$

with $\alpha_m = h_{13}(\hat{\rho}_m) - \frac{2h_{11}(\hat{\rho_m})}{\Delta\hat{\rho}^2}$, $\beta_m = \frac{h_{11}(\hat{\rho}_m)}{\Delta\hat{\rho}^2} + \frac{h_{12}(\hat{\rho}_m)}{2\Delta\hat{\rho}}$, $\gamma_m = \frac{h_{11}(\hat{\rho}_m)}{\Delta\hat{\rho}^2} - \frac{h_{12}(\hat{\rho}_m)}{2\Delta\hat{\rho}}$, $h^m_{NBI,i} = h_{NBI,i}(\hat{\rho}_m)$, $h^m_{EC} = h_{EC}(\hat{\rho}_m)$, $h^m_{BS,1} = h'_{BS}(\hat{\rho}_m)$, $h^m_{BS,2} = h_{BS}(\hat{\rho}_m)$. Since $\boldsymbol{u}_{aux}$ is the vector of virtual inputs, it is beneficial to rewrite the ODE in (12) in the form

$$\dot{\boldsymbol{\theta}}(t) = G_\eta(\boldsymbol{\theta}, t)u_\eta + G^*_{aux}(t)\boldsymbol{P}_{aux} + G_{BS}(\boldsymbol{\theta}, t)u_{BS}, \quad (16)$$

where $\boldsymbol{P}_{aux} = \{P_{NBI,1}, \ldots, P_{NBI,N_{NBI}}, P_{EC}\}$. In the above equation, the matrix $G^*_{aux}$ is defined such that it satisfies the constraint $G^*_{aux}\boldsymbol{P}_{aux} = G_{aux}\boldsymbol{u}_{aux}$. The goal of the controller designed in the following section is to choose $\boldsymbol{P}_{aux}$ such that the system tracks a target poloidal flux gradient $\bar{\boldsymbol{\theta}}$. For brevity of notation, the input $\boldsymbol{P}_{aux}$ will be represented by $\boldsymbol{u} = [u_1, \ldots, u_n]^T$ ($n = N_{NBI} + 1$) in the subsequent sections. Thus, the error equation that governs the evolution of $\tilde{\boldsymbol{\theta}} = \boldsymbol{\theta} - \bar{\boldsymbol{\theta}}$ takes the form

$$\dot{\tilde{\boldsymbol{\theta}}}(t) = f(\tilde{\boldsymbol{\theta}}, t) + g(\tilde{\boldsymbol{\theta}}, t)\boldsymbol{u}(t) \quad (17)$$

with $f = G_\eta u_\eta + G_{BS}u_{BS} - \dot{\bar{\boldsymbol{\theta}}}$, $g = G^*_{aux}$, $\boldsymbol{u} = \boldsymbol{P}_{aux}$.

Before proceeding to control synthesis, it is assumed that the attenuation or amplification of the effect of the auxiliary drives on the plasma evolution is always bounded. Such an assumption, which is typically valid in any given tokamak scenario, is formally stated as:

*Assumption 1:* At each time $t$, any $\boldsymbol{x} \in \mathbb{R}^n$, the function $g$ satisfies $0 < \epsilon \leq \|g(\boldsymbol{x}, t)\| \leq \bar{g}$, where $\|\cdot\|$ represents the induced 2-norm and $\epsilon, \bar{g} \in \mathbb{R}$ are constants.

## III. Control Synthesis

This section focuses on presenting the control law as well as the hypothesis required for establishing the stability and input-boundedness results. Suppose that $\check{\boldsymbol{u}} = [\check{u}_1, \ldots, \check{u}_n]^T$, $\hat{\boldsymbol{u}} = [\hat{u}_1, \ldots, \hat{u}_n]^T$ represent the vector of lower and upper saturation limits of the input $\boldsymbol{u}$, respectively. In other words, the physical constraints in the system ensure that $\check{u}_i \leq u_i \leq \hat{u}_i$ for all $i \in \{1, \ldots, n\}$ and all time $t$.

The proposed nonlinear control law is written as

$$\boldsymbol{u}(t) = \boldsymbol{u}_{off} - \boldsymbol{u}_{tr}(t), \quad (18)$$

where

$$\boldsymbol{u}_{off} := \frac{\check{\boldsymbol{u}} + \hat{\boldsymbol{u}}}{2}, \qquad \breve{u}_i := \left(\frac{\hat{u}_i - \check{u}_i}{2}\right) \quad (19)$$

$$\boldsymbol{u}_{tr}(t) := \begin{cases} A(\tilde{\boldsymbol{\theta}}(t), t)(s(\tilde{\boldsymbol{\theta}}(t), t))^T & \text{if } \|s(\tilde{\boldsymbol{\theta}}(t), t)^T\| \neq 0, \\ 0 & \text{if } \|s(\tilde{\boldsymbol{\theta}}(t), t)^T\| = 0, \end{cases} \quad (20)$$

$$A(\tilde{\boldsymbol{\theta}}, t) := diag\left(\alpha_1(\tilde{\boldsymbol{\theta}}, t) \ldots, \alpha_n(\tilde{\boldsymbol{\theta}}, t)\right), \quad (21)$$

$$\alpha_i(\tilde{\boldsymbol{\theta}}, t) := \frac{r_1(\tilde{\boldsymbol{\theta}}, t) + \sqrt{r_2(\tilde{\boldsymbol{\theta}}, t)^2 + \left(\breve{u}_i\|s(\tilde{\boldsymbol{\theta}}, t)^T\|\right)^4}}{\|s(\tilde{\boldsymbol{\theta}}, t)^T\|^2\left[1 + \sqrt{1 + \left(\breve{u}_i\|s(\tilde{\boldsymbol{\theta}}, t)^T\|\right)^2}\right]} \quad (22)$$

$$s(\tilde{\boldsymbol{\theta}}, t) := \tilde{\boldsymbol{\theta}}^T g(t), \quad (23)$$

$$r_1(\tilde{\boldsymbol{\theta}}, t) := r(\tilde{\boldsymbol{\theta}}, t) + \mu\|2\tilde{\boldsymbol{\theta}}\|\underbrace{\left(\frac{\|2\tilde{\boldsymbol{\theta}}\|}{\|2\tilde{\boldsymbol{\theta}}\| + \lambda}\right)}_{<1}, \quad (24)$$

$$r_2(\tilde{\boldsymbol{\theta}}, t) := r(\tilde{\boldsymbol{\theta}}, t) + \mu\|2\tilde{\boldsymbol{\theta}}\|, \quad (25)$$

$$r(\tilde{\boldsymbol{\theta}}, t) := \tilde{\boldsymbol{\theta}}^T f^*(t), \quad (26)$$

$$f^*(\tilde{\boldsymbol{\theta}}, t) := f(\tilde{\boldsymbol{\theta}}, t) + g(\tilde{\boldsymbol{\theta}}, t)\boldsymbol{u}_{off}(t), \quad (27)$$

for all $i \in \{1, \ldots, n\}$. The constants $\mu > 0$ and $\lambda > 0$ in the above definitions are adjustable parameters. The term $\boldsymbol{u}_{off}$ in the control law is the constant offset term that accounts for any nonsymmetry in the actuator constraints. On the other hand, the transient term $\boldsymbol{u}_{tr}$ depends on the state error $\tilde{\boldsymbol{\theta}}$. Since $\alpha_i$ is undefined when $\|s(\tilde{\boldsymbol{\theta}}(t), t)^T\| = 0$, the condition on $\|s(\tilde{\boldsymbol{\theta}}(t), t)^T\|$ in (20) ensures that the control law given by (18) is mathematically feasible.

As it will be shown below, the satisfaction of the input bounds and the stability of the closed-loop system demand the state to evolve in a "controllable region." Such "controllable region" $\Pi_t$ is defined as the set

$$\Pi_t := \left\{\tilde{\boldsymbol{\theta}} \in \mathbb{R}^n : \max\{|r_1(\tilde{\boldsymbol{\theta}}, t)|, |r_2(\tilde{\boldsymbol{\theta}}, t)|\} \leq \breve{u}\|s(\tilde{\boldsymbol{\theta}}, t)^T\|\right\}, \quad (28)$$

$$\breve{u} := min\left\{\breve{u}_i \text{ for } 1 \leq i \leq n\right\}. \quad (29)$$

As it is clear from the above definition, the set $\Pi_t$ evolves with time since the nonlinear functions $f$ and $g$ in the error equations (17) and hence the nonlinear terms $r_1$, $r_2$, $s$ also vary with time.

The following theorem establishes that the closed-loop system's equilibrium at the origin is asymptotically stable as long at the state is contained in the set $\Pi_t$. The function variables $\tilde{\boldsymbol{\theta}}$ and $t$ are dropped in the following theorem and all subsequent analysis. In addition, the subscript $i$ represents the $i^{th}$ element of any given vector.

*Theorem 1:* The control input $\boldsymbol{u} = [u_1, \ldots, u_n]^T$ defined in (18) makes the equilibrium at the origin of the closed-loop system uniformly asymptotically stable as long as the state $\tilde{\boldsymbol{\theta}}(t)$ is contained in the set $\Pi_t$ for all time $t$.

*Proof:* Consider the Lyapunov function $V = \frac{1}{2}\tilde{\boldsymbol{\theta}}^T\tilde{\boldsymbol{\theta}}$. Its time derivative is given by

$$\dot{V} = \tilde{\boldsymbol{\theta}}^T\left[f + g\boldsymbol{u}\right] = \tilde{\boldsymbol{\theta}}^T f^* + \tilde{\boldsymbol{\theta}}^T g\left(-As^T\right) \leq r - \hat{\alpha}\|s^T\|^2,$$

where we have used (17), (18), (21), (23), (26), (27), and where $\hat{\alpha}$ is defined as $\hat{\alpha} := min_i\alpha_i$ for all $i \in \{1, \ldots, n\}$. Let $\breve{\breve{u}}$ be the value of $\breve{u}_i$ corresponding to the element in matrix $A$ that attains $\hat{\alpha}$. By using (22), it can be shown that the time derivative of the Lyapunov function is bounded by

$$\begin{aligned}\dot{V} &\leq r - \|s^T\|^2\left[\frac{r_1 + \sqrt{(r_2)^2 + (\breve{\breve{u}}\|s^T\|)^4}}{\|s^T\|^2\left[1 + \sqrt{1 + (\breve{\breve{u}}\|s^T\|)^2}\right]}\right] \\ &\leq \underbrace{\frac{r\left[\sqrt{1 + (\breve{\breve{u}}\|s^T\|)^2}\right] - \sqrt{(r_2)^2 + (\breve{\breve{u}}\|s^T\|)^4}}{\left[1 + \sqrt{1 + (\breve{\breve{u}}\|s^T\|)^2}\right]}}_{I} \\ &\quad - \underbrace{\frac{\mu\|2\tilde{\boldsymbol{\theta}}\|^2}{(\|2\tilde{\boldsymbol{\theta}}\| + \lambda)\left[1 + \sqrt{1 + (\breve{\breve{u}}\|s^T\|)^2}\right]}}_{II},\end{aligned} \quad (30)$$

where we have used the fact that $r - r_1 \leq 0$ from (24). Since the states are contained in the set $\Pi_t$, the inequality

$$|r_2| \leq \breve{u}\|s^T\| \quad (31)$$

holds at all time $t$. Furthermore, since $\breve{u}$ is the minimum of $\breve{u}_i$ for $1 \leq i \leq n$ (by definition) and $\breve{\breve{u}}$ is equal to $\breve{u}_j$ where $j$ corresponds to the index of the minimum of $\hat{\alpha}_i$ (also by definition), we conclude that $\breve{u} \leq \breve{\breve{u}}$. Now, we split the inequality given in (31) and consider two different cases.

*Case (i):* If $-\breve{\breve{u}}\|s^T\| \leq -\breve{u}\|s^T\| \leq r_2 \leq 0$, we conclude from (25) that $r = r_2 - \mu\|2\tilde{\boldsymbol{\theta}}\| \leq 0$ since $\mu > 0$ by assumption. This implies that the term $I$ in (30) satisfies $I \leq 0$, which in turn implies that $\dot{V} \leq -II < 0$.

*Case (ii):* If $0 < r_2 \leq \breve{u}\|s^T\| \leq \breve{\breve{u}}\|s^T\|$, the inequality

$$-\sqrt{(r_2)^2 + (\breve{\breve{u}}\|s^T\|)^4} \leq -r_2\sqrt{1 + (\breve{\breve{u}}\|s^T\|)^2} \tag{32}$$

holds. This implies that $I \leq 0$ since $r - r_2 \leq 0$ by definition given in (25). Thus, $\dot{V} \leq -II < 0$.

Thus, the time derivative of the Lyapunov function satisfies the inequality $\dot{V} \leq -II < 0$ in both the cases. Note that $II$ is a function of time $t$ and state $\tilde{\boldsymbol{\theta}}$, where the explicit dependence on time $t$ comes because of the term $s$ in $II$. From Assumption 1, we have $\|s^T\| \leq \|g(\tilde{\boldsymbol{\theta}}, t)^T\|\|\tilde{\boldsymbol{\theta}}\| \leq \bar{g}\|\tilde{\boldsymbol{\theta}}\|$. As a result, the inequality

$$\dot{V} \leq -II \leq -\frac{\mu\|2\tilde{\boldsymbol{\theta}}\|^2}{(\|2\tilde{\boldsymbol{\theta}}\| + \lambda)\left[1 + \sqrt{1 + (\breve{\breve{u}}\bar{g}\|\tilde{\boldsymbol{\theta}}\|)^2}\right]} < 0 \tag{33}$$

holds. In the above inequality, $\breve{\breve{u}} := max\{\breve{u}_i, 1 \leq i \leq n\}$. Thus, the time derivative of the Lyapunov function is bounded from above by a negative definite function. Now, the result of the theorem follows directly from the Lyapunov stability theorem [14]. ■

The following theorem shows that each element of the control input vector satisfies the saturation constraint as long as the state is contained in the "controllable region."

*Theorem 2:* The control input $\boldsymbol{u} = [u_1, \ldots, u_n]^T$ defined by (18) satisfies the nonsymmetric individual actuator constraints $\breve{u}_i \leq u_i \leq \hat{u}_i$ for all $i \in \{1, \ldots, n\}$ and all time $t$ if the state $\tilde{\boldsymbol{\theta}}(t)$ is contained in the set $\Pi_t$ for all time $t$.

*Proof:* By exploiting the structure of the matrix $A(\tilde{\boldsymbol{\theta}}(t), t)$ in (21), the absolute value of $i^{th}$ transient input $|u_{tr,i}|$, defined in (20), is bounded from above by

$$|u_{tr,i}| \leq |\alpha_i|\,|s_i| \leq \frac{|r_1 + \sqrt{(r_2)^2 + (\breve{u}_i\|s^T\|)^4}|}{\|s^T\|^2\left[1 + \sqrt{1 + (\breve{u}_i\|s^T\|)^2}\right]}\|s^T\|.$$

From the assumption that $\tilde{\boldsymbol{\theta}}$ is contained in the set $\Pi_t$, defined in (28), we have $|r_1| \leq \breve{u}\|s^T\| \leq \breve{u}_i\|s^T\|$ and $|r_2| \leq \breve{u}\|s^T\| \leq \breve{u}_i\|s^T\|$. Then,

$$|u_{tr,i}| \leq \frac{|r_1| + \sqrt{(r_2)^2 + (\breve{u}_i\|s^T\|)^4}}{\|s^T\|\left[1 + \sqrt{1 + (\breve{u}_i\|s^T\|)^2}\right]} \tag{34}$$

$$\leq \frac{\breve{u}_i\|s^T\|\left[1 + \sqrt{1 + (\breve{u}_i\|s^T\|)^2}\right]}{\|s^T\|\left[1 + \sqrt{1 + (\breve{u}_i\|s^T\|)^2}\right]} = \breve{u}_i. \tag{35}$$

It is evident from (18) that $|u_{tr,i}| = |u_i - u_{off,i}| \leq \breve{u}_i$. Using the definitions of $u_{off,i}$ and $\breve{u}_i$ in (19) and (29), respectively, and rearranging the terms will give the inequality $\breve{u}_i \leq u_i \leq \hat{u}_i$. ■

The hypothesis of Theorem 1 and Theorem 2 that the state $\tilde{\boldsymbol{\theta}}(t)$ is contained in the set $\Pi_t$ cannot be checked a priori (before controller implementation). However, if there exists an open ball $B_\epsilon(\mathbf{0})$ of radius $\epsilon$ centered at the origin $\mathbf{0}$ such that $B_\epsilon(\mathbf{0}) \subseteq \cap_{t\geq 0}\Pi_t$ and the initial condition $\tilde{\boldsymbol{\theta}}(0)$ is such that $\tilde{\boldsymbol{\theta}}(0) \in B_\epsilon(\mathbf{0})$, then the control input $\boldsymbol{u} = [u_1, \ldots, u_n]^T$ defined in (18) satisfies the nonsymmetric individual actuator constraints $\breve{u}_i \leq u_i \leq \hat{u}_i$ for all $i \in \{1, \ldots, n\}$ and all time $t$ and makes the equilibrium at the origin of the closed-loop system uniformly asymptotically stable.

### A. Remarks on Controller Implementation

(i) It is often difficult to write down an explicit equation for the elements of the set $\Pi_t$ in most practical applications like plasma profile control. However, numerical algorithms can be used to search for elements of the state space that are contained in the set $\Pi_t$ since this search can be carried out offline before the implementation of the controller. To get an estimate of the open ball $B_\epsilon(\mathbf{0})$ in the case of nonautonomous systems, the sets $\Pi_t$ can be computed at discrete time steps and the regions of overlap can be determined. Detailed discussion of methods and algorithms to compute these sets is beyond the scope of the current paper.

(ii) From the definition of the set $\Pi_t$ (given in (28)), it is clear that the size of the "controllable region" depends on the smallest saturation limit $\breve{u}$. One can scale the inputs such that all actuators have similar saturation limits. This in turn can increase the "controllable region" in certain cases.

(iii) By definition, the set $\Pi_t$ depends on the time evolution of the target $\dot{\bar{\boldsymbol{\theta}}}$. Generally, for the problem of current profile control in tokamaks, the target profile depends on time. However, in certain tokamak scenarios, the target during the flat-top phase is fixed. In such cases, the "controllable region" depends only on the dynamics of the tokamak under consideration.

## IV. Numerical Simulation

This section focuses on closed-loop simulations for a DIII-D tokamak scenario. The target for the simulations was generated using data from the DIII-D shot 147634. The simulations considered three noninductive current drives (two NBI and one ECH&CD) with 41 finite-difference nodes. The grey background in all the figures shows when the controller is active. In the simulations, the line-average electron density $\bar{n}_e$ and the plasma current $I_p$ are adopted from the DIII-D shot 147634. The total power $P_{tot}$ used in the simulations is the sum of the feedforward inputs (shown in Figure 2). Furthermore, the controller parameters $\mu > 0$ and $\lambda > 0$ are set as $\mu = 1 \times 10^{-5}$ and $\lambda = 1$, respectively. The controller bounds of the three noninductive current drives used in the simulations are $0 \leq u_1 \leq 15\ MW$, $0 \leq u_2 \leq 15\ MW$, $0 \leq u_3 \leq 7.5\ MW$. Note that $u_1$, $u_2$, $u_3$ correspond to $P_{NBI,1}$, $P_{NBI,2}$ and $P_{EC}$, respectively. In the simulations, the ECH&CD power is scaled by a factor of 2. As a result, the upper bound $\hat{u}_3$ and hence $\breve{u}$, defined in (29),

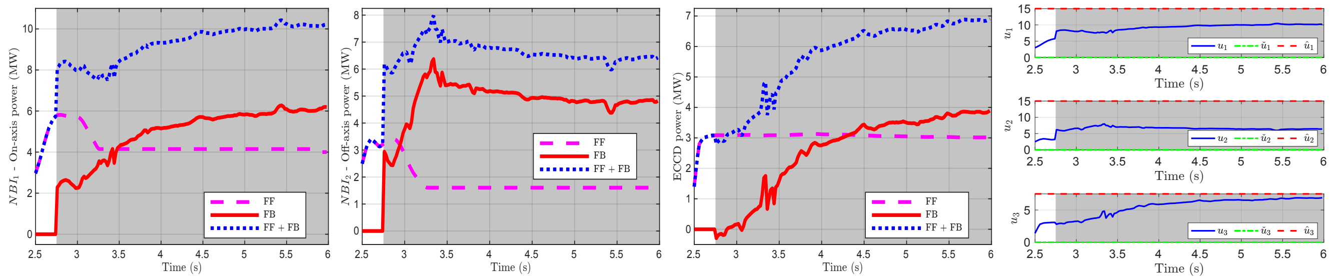


Fig. 2: From left to right: $P_{NBI_1}$; $P_{NBI,2}$; $P_{EC}$; Individual inputs with bounds (Top - $|u_1|$, Center - $|u_2|$, Bottom - $|u_3|$)

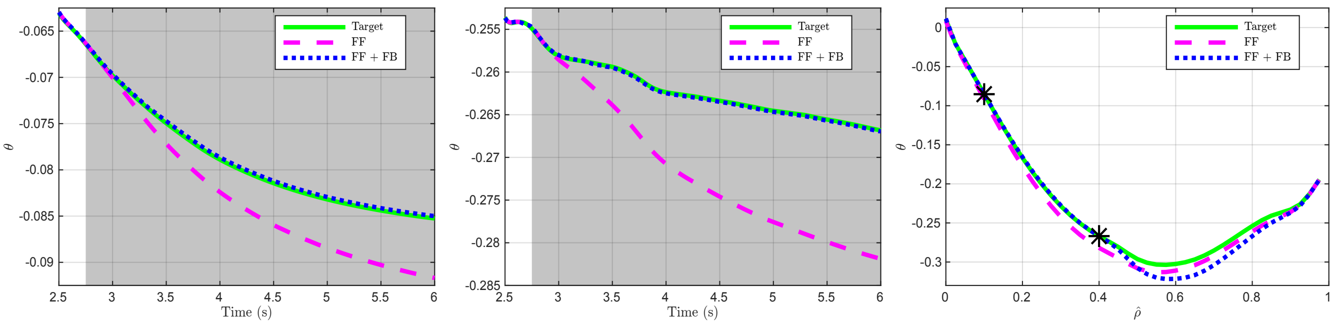


Fig. 3: Poloidal flux gradient: Left - $\boldsymbol{\theta}(0.1,\cdot)$, Center - $\boldsymbol{\theta}(0.4,\cdot)$, Right - $\boldsymbol{\theta}(\cdot,6s)$

are also scaled by a factor of 2 to increase the size of the "controllable region." Furthermore, two spatial nodes where the NBI and ECH&CD current depositions are significant ($\hat{\rho}=0.1$ and $\hat{\rho}=0.4$) are considered for control.

Figure 2 shows the feedback inputs generated by the controller along with the corresponding feedforward values. The figure also shows the absolute value of each of the feedback inputs. The inputs satisfy the saturation limits at all times $t$. The effectiveness of the controller is evident from Figure 3. The figure shows the poloidal flux gradient values at the two control nodes. It is clear that the controller can track the given targets at the two control points. In addition, Figure 3 also shows the whole poloidal flux gradient profile at $t=6$ seconds. The profile at the end of the simulation matches the target at approximately all $\hat{\rho}\in[0,0.4]$.

## V. Conclusion and Future Work

This work presents a Lyapunov-based nonlinear feedback control approach that can guarantee bounds on the individual components of a nonlinear system's inputs. In particular, the control algorithm was developed for the current profile control problem in tokamaks. The proposed controller inherently accounts for the individual nonsymmetric saturation limits in the input formula and does not rely on computationally expensive optimization techniques. A detailed analysis of the tokamak model assumptions necessary for implementing the controller is presented. Furthermore, the controller's stabilization properties and input-bound guarantees are discussed rigorously. Finally, the validity of the theoretical results is shown through simulations for a DIII-D tokamak scenario. This work's potential future extensions include testing the controller in higher fidelity tokamak simulators before performing experiments on a real tokamak.

## References


[1] J. Wesson and D. J. Campbell, *Tokamaks*. Oxford university press, 2011, vol. 149.

[2] A. Pajares and E. Schuster, "Central safety factor control in DIII-D using neutral beam injection and electron cyclotron launchers in zero input-torque scenarios," in *2017 IEEE Conference on Control Technology and Applications (CCTA)*, Aug. 2017, pp. 1460–1465.

[3] M. D. Boyer *et al.*, "Backstepping Control of the Toroidal Plasma Current Profile in the DIII-D Tokamak," *IEEE Transactions on Control Systems Technology*, vol. 22, no. 5, pp. 1725–1739, Sep. 2014.

[4] N. T. Vu *et al.*, "Plasma internal profile control using IDA-PBC: Application to TCV," *Fusion Engineering and Design*, vol. 123, pp. 624–627, Nov. 2017.

[5] W. Wehner *et al.*, "Optimal current profile control for enhanced repeatability of L-mode and H-mode discharges in DIII-D," *Fusion Engineering and Design*, vol. 123, pp. 513–517, Nov. 2017.

[6] M. D. Boyer *et al.*, "First-principles-driven model-based current profile control for the DIII-D tokamak via LQI optimal control," *Plasma Physics and Controlled Fusion*, vol. 55, no. 10, p. 105007, Sep. 2013.

[7] B. Mavkov *et al.*, "Experimental validation of a Lyapunov-based controller for the plasma safety factor and plasma pressure in the TCV tokamak," *Nuclear Fusion*, vol. 58, no. 5, p. 056011, Mar. 2018.

[8] E. Maljaars *et al.*, "Profile control simulations and experiments on TCV: A controller test environment and results using a model-based predictive controller," *Nuclear Fusion*, vol. 57, no. 12, p. 126063, Oct. 2017.

[9] A. Pajares and E. Schuster, "Robust Nonlinear Control of the Minimum Safety Factor in Tokamaks," in *5th IEEE Conference on Control Technology and Applications*, 2021.

[10] S. T. Paruchuri *et al.*, "Minimum safety factor control in tokamaks via optimal allocation of spatially moving electron cyclotron current drive," in *60th IEEE Conference on Decision and Control*, 2021.

[11] N. H. El-Farra and P. D. Christofides, "Bounded robust control of constrained multivariable nonlinear processes," *Chemical Engineering Science*, vol. 58, no. 13, pp. 3025–3047, Jul. 2003.

[12] F. L. Hinton and R. D. Hazeltine, "Theory of plasma transport in toroidal confinement systems," *Reviews of Modern Physics*, vol. 48, no. 2, pp. 239–308, Apr. 1976.

[13] J. E. Barton *et al.*, "Physics-based control-oriented modeling of the safety factor profile dynamics in high performance tokamak plasmas," in *52nd IEEE Conference on Decision and Control*, Dec. 2013, pp. 4182–4187.

[14] H. K. Khalil, *Nonlinear Systems*, 3rd ed. Pearson, 2002.